Ionic Liquid-Mediated Route to Atomic Layer Deposition of Tin(II) Oxide via a C-C Bond Cleavage Ligand Modification Mechanism

Jingwei Shi, ¹ Seunggi Seo, ^{1,3} Nathaniel J. Schuster, ² Hyungjun Kim, ³ Stacey F. Bent^{1,*}

¹Department of Chemical Engineering, Stanford University, Stanford, California 94305, United States

²Department of Chemistry, Stanford University, Stanford, California 94305, United States

³School of Electrical and Electronic Engineering, Yonsei University, Seoul, 03722, Republic of Korea

*Corresponding Author: sbent@stanford.edu

Abstract

Atomic layer deposition (ALD) is a technologically important method to grow thin films with high conformality and excellent thickness control from vapor phase precursors. The development of new thermal ALD processes can be limited by precursor reactivity and stability: reaction temperature and precursor design are among the few variables available to achieve higher reactivity, unlike in solution synthesis where the use of solvent and/or a catalyst can promote a desired reaction. To bridge this synthesis gap between vapor and solution, we demonstrate the use of an ultrathin coating layer of a vapor-phase compatible solvent—an ionic liquid (IL)—onto our growth substrate to perform ALD of SnO. Successful SnO deposition is achieved using tin acetylacetonate and water, a process that otherwise would require a stronger counter-reactant such as ozone. The layer of IL allows a solvent-mediated reaction mechanism to take place on the growth substrate. We report a growth per cycle of 0.67 Å/cycle at a deposition temperature of 100 °C in an IL comprised of 1-ethyl-3-methylimidazolium hydrogen sulfate. Characterization of the ALD films confirms the SnO film composition, and ¹H and ¹³C NMR are used to probe the solvent-mediated ALD reaction, suggesting a solvent-mediated additionelimination type mechanism forming acetone and acetate. Density functional theory calculations show that the ionic liquid solvent is beneficial to the proposed solvent-mediated mechanism by lowering the C-C bond cleavage energetics of acetylacetonate compared to the vapor phase. A general class of ligand-modification reactions for thermal ALD is thus introduced in this work.

Introduction

Atomic layer deposition (ALD) has been and continues to be the subject of significant research effort for fields such as semiconductor manufacturing, ¹⁻⁴ catalysis, ⁵⁻⁹ energy storage, ¹⁰⁻ ¹⁴ and photovoltaics. ^{15,16} ALD is a vapor-phase vacuum deposition technique that utilizes alternating self-limiting gas-surface reactions to grow thin films on solid substrates. Under a specific range of deposition temperatures, termed the ALD growth window, the growth per cycle (GPC) is approximately constant. The technique allows for the atomic scale deposition and manipulation of inorganic materials. A large proportion of ALD research has focused on the development of new processes: growing new metal oxides, ^{17–20} nitrides, ^{21–23} sulfides, ^{24–27} etc., and even doped, ternary, and quaternary compounds.²⁸ In many of these reports, the deposition conditions and ALD window are reported but are not the main focus of the study. At the same time, there is demand in the field to extend the processing conditions of a particular ALD process, i.e., using less reactive or oxidative precursors or lower deposition temperature. This type of study is worthwhile since the applicability of ALD can be limited by either the deposition temperature (such as for solar cell applications¹⁶ or growth on polymeric substrates^{29–31}) or precursor incompatibilities with the system (e.g., if highly oxidizing counter-reactants like ozone are not compatible with the substrate).

The gas-surface reaction mechanisms in ALD can generally be classified into four types:³² 1) ligand exchange, 2) dissociation, 3) association, and 4) oxidation. Of the four general classes, only oxidation type mechanisms change the identity of the ligands on reactants; in the first three classes of reactions, ligands simply swap between the reactants or with the surface.

When viewed in the larger context of known chemical reactions mechanisms, it is clear that ALD reactions comprise just a very narrow subset. For one, most ALD reactions do not involve

catalysts nor solvents. This constraint precludes the vast number of solution- and catalystmediated reactions from being utilized in ALD. In order to develop new ALD processes and extend the processing conditions of existing ones, tapping into these solution-mediated reactions is a potentially fruitful strategy.

In a previous study, we investigated the use of ultrathin coatings (~100 Å) of ionic liquid (IL) as vacuum-compatible solvents to aid in the deposition of molecular layer deposition (MLD) films.³³ We hypothesized that the IL solvent layer changed the energetics of the surface reaction to enable the MLD of polyetherketoneketone (PEKK), which had previously not been deposited as a thin film in vapor phase, even under CVD conditions. Ionic liquids are salt melts that possess extremely low vapor pressures, nearing 100 pTorr for select ILs at room temperature,³⁴ making them compatible with vacuum systems. ILs have been the subject of research in the field of chemistry as a potential green solvent.^{35,36} As a class of solvents, ILs are versatile because they can have differing polarities, Bronsted acidity/basicity, and Lewis acidity/basicity depending on the cation/anion pair chosen. In fact, ILs have already been used as solvents in vapor-phase environments to perform catalytic surface reactions in the field of supported ionic liquid phase (SILP) catalysis.^{37,38}

We look to extend the use of ionic liquids to ALD in this work, focusing on the process of tin acetylacetonate with water as the counter-reactant. Traditionally, metal acetylacetonates have been used in many ALD processes to form both metal and metal oxide thin films, but notably, the deposition of metal oxides typically requires ozone^{39–45} or oxygen^{46–50} at elevated deposition temperatures >200 °C. A couple exceptions in literature are the In₂O₃⁴⁴ and Ga₂O₃⁵¹ processes from indium acetylacetonate and gallium acetylacetonate, respectively, with water, for which the process deposition temperature is 350 °C for gallium oxide⁵¹ and 200 °C for indium

oxide.⁴⁴ Furthermore, for the indium oxide process, there are conflicting reports about whether the process is even possible.^{44,52} On the other hand, in the solution-phase synthesis of metal oxide nanoparticles with metal acetylacetonates, the reaction conditions are more mild,^{53–56} with reported reactions occurring with non-oxidizing nucleophiles such as alcohols⁵³ or amines.⁵⁴ This result suggests that there may be a solvent-mediated mechanism with acetylacetonates that allows for its reactivity with less harsh counter-reactants that is not accessible in the vapor-phase, motivating our investigation of this system using IL-ALD.

In this study, we investigate the tin oxide ALD process using tin acetylacetonate, aiming to reduce both the deposition temperature as well as the oxidizing nature of the counter precursor from ozone to water, by using 1-ethyl-3-methylimidazolium hydrogen sulfate as the IL layer to promote the corresponding solvent-mediated surface reaction. Tin acetylacetonate has previously been reported to react with ozone, but not with oxygen nor water, ³⁹ and no SnO ALD process has yet been shown between tin acetylacetonate and water. However, we demonstrate in this work that with the assistance of an ionic liquid solvent layer, tin acetylacetonate can react with water at temperatures as low as 100 °C with a GPC of ~0.7 Å/cycle.

Methods

Description of Materials. 1-ethyl-3-methylimidazolium hydrogen sulfate (EMIM HSO₄) was purchased from Sigma-Aldrich and used as received. Tin(II) acetylacetonate (Sn(acac)₂) was purchased from Strem Chemicals and used as received. All reagents were stored in a nitrogen-purged glovebox until use. Films were deposited on n-doped (100) Si substrates with 15 Å native oxide purchased from PureWafers.

Surface Treatment. Prior to ALD deposition, silicon substrates were cleaned by sonication in deionized water for 10 min. Next, the substrates were cleaned for 30 min in a Novascan PSD Series digital UV ozone system to remove remaining organic contamination. The Si substrates were coated with an ultrathin layer of ionic liquid via spin-coating at 3000 rpm for 30 sec. A 1% (w/w) solution of EMIM HSO₄ in acetone was prepared as the stock spin-coating solution. Serial dilutions were then prepared from this stock solution to achieve control over the thickness of the IL coating layer according to the spin-curve shown in SI Figure S1. The standard IL layer thickness was ~165 Å.

Description of Reactor and Atomic Layer Deposition Conditions. Once the IL layer was deposited onto Si substrates, the wafers were introduced into a hot-wall flow reactor, similar in design to one described previously⁵⁷ and pumped by a Leybold Trivac rotary vane pump with a base pressure of 130 mTorr. Sufficient nitrogen was flowed in the reactor to maintain a working pressure of 2.5 torr for optimal purging conditions. The transfer lines and bubbler containing the precursor Sn(acac)₂ were heated to 50 °C to achieve sufficient vapor pressure, and those containing the water counter-reactant were kept at room temperature. The walls of the deposition chamber were heated to 100 °C. An ALD cycle consisted of two temporally separated subcycles using an AB dosing scheme, in which Sn(acac)₂ and water were alternatively introduced into the reactor. Each ALD dose subcycle consisted of several steps: (1) predose pump, in which nitrogen flow was stopped, and the chamber was allowed to pump down for 30 s; (2) dose, in which a pneumatic ALD valve was opened to introduce the chemical species into the reactor while both nitrogen flow and pump were closed off; (3) soak, in which the chemical species inlet, nitrogen flow, and pump were closed off to allow the dosed vapor to remain in the chamber to reactor; and (4) purge, in which both nitrogen and pump were opened to the reactor

to purge away all reaction species. Typical dose/soak/purge times for $Sn(acac)_2$ and water were 1 s/10 s/120 s and 0.5 s/10 s/120 s respectively.

Characterization Techniques. Surface morphology and conformality of the IL layers were probed with atomic force microscopy (AFM) using a Park NX10 atomic force microscope. The root-mean-square (RMS) roughness (R_q) was calculated using the root-mean-squared deviation of the surface height from the mean. The thicknesses of the IL layers as well as subsequent SnO ALD films were measured using variable angle spectroscopic ellipsometry (VASE) using a J. A. Woollam Co. α -SE spectroscopic ellipsometer with a spectral range of 300-900 nm. Thickness of SnO ALD films were probed by VASE after first sonicating the substrate in DI water to remove the IL layer.

X-ray photoelectron spectroscopy was performed by a PHI 5000 VersaProbe III spectrometer with a monochromatic Al Kα X-ray source at 1486 eV. The X-ray beam spot size was 200 x 200 μm, at 100 W and 20 kV. Survey scans were taken at 224 eV pass energy in triplicate and at 1 eV/step resolution with 20 ms/step. High-resolution scans were collected at 55 eV pass energy for five scans at 0.2 eV/step resolution with 20 ms/step. Valence band spectra were collected at 55 eV pass energy for thirty scans at 0.2 eV/step resolution with 20ms/step. Depth profile experiments were performed with an Ar ion gun to sputter and remove material while periodically collecting XPS scans.

¹H and 13C nuclear magnetic resonance (NMR) spectra were collected on a Bruker NMR Spectrometer at 400 MHz and 101 MHz, respectively. The measurement sample was prepared by first adding 1 mL of Sn(acac)₂ precursor to 1 g of EMIM HSO₄ solvent inside of a glovebox. The vial was taken out of the glovebox and immediately 2 mL of D₂O was added to the solution. A yellow-white milky suspension immediately formed upon addition of the D₂O. The reaction

mixture was allowed to react fully in a furnace while the vial was capped and sealed with parafilm at 80 °C for 2 hr. Next, the suspension was filtered cleanly through a 0.45 micron Nylon filter into a NMR tube that was baked for 10 min at 150 °C prior. The NMR spectra were recorded at 298 K.

Density Functional Theory (DFT) Calculations. All the DFT calculations were performed using the Gaussian 16 suite of programs.⁵⁸ Becke's three-parameter hybrid functional (B3LYP)^{59,60} and Def2-TZVP basis set^{61,62} were used. For dispersion correction, Grimme's dispersion with Becke-Johnson damping (GD3BJ) was applied.^{63,64} Gaussian 16 software offers a calculation option with solvent which is performed by placing the molecules within the solvent reaction field. The Polarizable Continuum Model (PCM) using the integral equation formalism variant (IEFPCM) is the default method for solvation.⁶⁵ However, our proposed addition-elimination mediated reaction mechanism could be affected by the partial charge of the IL molecules, which is not captured well by mean field models such as PCM. So, we simulated here the presence of the IL by using an individual EMIM-HSO4 complex interacting with the either the precursor or counter-reactant molecule. The thermochemical values such as thermal energy (E), enthalpy (H), entropy (S), and Gibbs free energy(G) were considered by using vibrational frequency calculations. The temperature was set to 100 °C for this study.

Results and Discussion

Characterization of the EMIM HSO₄ IL Layer. The IL layer should possess two properties for the ionic liquid assisted ALD process to be feasible:³³ (1) The IL must not evaporate under the deposition conditions in the reactor and (2) the IL must wet the Si substrate to form a continuous wetting layer. Ionic liquids possess extremely low vapor pressures compared to

conventional solvents, which enables their use in our low-vacuum deposition chamber and in principle should ensure their stability at the reactor pressures.^{34–36,66,67} To confirm the thermal stability of the IL layer, we investigated both its thickness by VASE and its composition by XPS. The IL layer was deposited onto Si substrates via spin-coating as described in the Methods section then loaded into the reactor. After leaving the IL-coated substrates under reaction conditions (100 °C stage temperature, 2.5 torr working pressure), the thickness remained unchanged via VASE. XPS of the IL layer after the stability tests in SI Figure S2 also revealed that the nominal elemental composition did not change, which suggests its thermal stability.

Next, we examined the wetting of the IL on the substrate. Good wetting behavior for the IL is necessary because it enables the solvent to be a uniform thickness across the entire substrate. Because we hypothesize that the IL solvent layer is necessary for our solvent-mediated deposition process, if the IL layer is not conformal, the subsequent IL-ALD of the SnO film may also not be conformal. We confirmed the 2d wetting behavior of the IL layer on the Si substrate using AFM, by which we characterized the conformality of the IL films on the Si substrate using the RMS roughness metric. AFM results are shown in SI Figure S3. The IL layer possessed an RMS (Rq) roughness of 3 Å, which is a value relatively close to that of the underlying Si substrate (1 Å for Si). In our previous investigation, 33 we show that a poorly wetting IL shows visible de-wetting with an RMS roughness of 31 nm, which is 2 orders of magnitude more rough. Thus, we conclude that the IL layer is wetting the surface in a 2D continuous manner, as desired.

As described in Methods, the IL layer was removed prior to any characterization of the SnO film itself via sonication in DI water. However, we note that our prior work on IL-MLD³³ suggested that increasing the reactor wall temperature to raise the vapor pressure of the IL is another viable option to removing the IL layer in-situ via purging.

SnO ALD growth characterization. Literature on Sn(acac)₂ reported that tin acetylacetonate does not react with oxygen nor water at deposition temperatures below 375 °C in a traditional ALD process,³⁹ but rather is only reactive with ozone to deposit SnO₂ films at a growth per cycle (GPC) of 1 Å /cycle.³⁹ Hence, we do not expect growth to occur with Sn(acac)₂ and water in control experiments without an IL.

We investigated the growth characteristics of the SnO ALD process with Sn(acac)₂ and water both in the presence of the IL layer and without the IL. For these studies, the thickness of the deposited film under both conditions was measured by VASE. The results of the growth characterization studies are shown in Figure 1, as a function of the Sn(acac)₂ and water dose time, the number of ALD cycles, and IL thickness. Saturation studies were performed in order to confirm the self-limiting nature of the surface reaction. The saturation curves shown in Figure 1a, b reveal that without the IL layer (data shown in red), the deposition rate is extremely low, ~0.07 Å/cycle. However, for substrates coated with the EMIM HSO₄ IL layer, Sn(acac)₂ is able to react with water, leading to GPC at saturation of ~0.7 Å/cycle. Saturation of the GPC is observed for both Sn(acac)₂ and water, which confirms the self-limiting nature of the IL-ALD process. The GPC was also studied as a function of number of ALD cycles: Figure 1c shows the growth curve for IL-ALD and traditional ALD. The results reveal linear growth behavior in IL for at least 200 cycles with a GPC of 0.67 Å /cycle extracted from a least squares fit. In contrast, a lack of growth is observed on bare Si, with the film thickness never exceeding 7 Å even as the cycle number increases to 200 cycles, which agrees with previous reports on the standard thermal process.

Finally, as in our previous study on IL-MLD, 33 we investigated how the GPC varies with the thickness of the IL layer, summarized in Figure 1d. It is conceivable that the presence of the IL layer could hinder the effective purging of by-products, which would lead to CVD-like growth. This would be detected by a monotonic increase of the GPC with respect to IL layer thickness. As shown in Figure 1d, three GPC regimes are observed. There is a region in which the GPC of the IL-ALD process is constant at ~0.7 Å/cycle, between 120 – 200 Å of IL. At IL thicknesses larger than this window, the GPC increases significantly to ~3 Å/cycle. We have hypothesized in previous work that the cause of this rapid increase in the GPC in IL-ALD is due to insufficient purging at higher IL thicknesses, leading to CVD-like behavior, and we propose the same explanation here.³³ There are also some notable features in the data when using IL thicknesses below 120 Å: at IL thicknesses smaller than this value, the growth increases monotonically from a value of 0 Å/cycle with no IL to 0.7 Å/cycle at 120 Å. We attribute this behavior to artifacts arising from insufficient wetting of the surface at the lower IL thicknesses. Post-deposition, these thinner IL layer showed signs of de-wetting from the substrate; as we hypothesized above, the wetting of the IL layer is crucial to the IL-ALD process and the conformal growth of the ALD film. Furthermore, the nano-confinement effect of the IL adsorption on a solid substrate may affect the ability of these thinner IL layers to act as a solvent. 68–71 This phenomenon arises as the strongly interacting ionic liquid forms a solid-like phase near the surface of the substrate, which reduces its degrees of freedom, leading to loss of certain bulk-phase, liquid-like properties such as solvation strength and conductivity.⁶⁸ On the basis of the results in Figure 1d, we chose to use an IL thickness of 165 Å for all other experiments because it is in the region where GPC is constant.

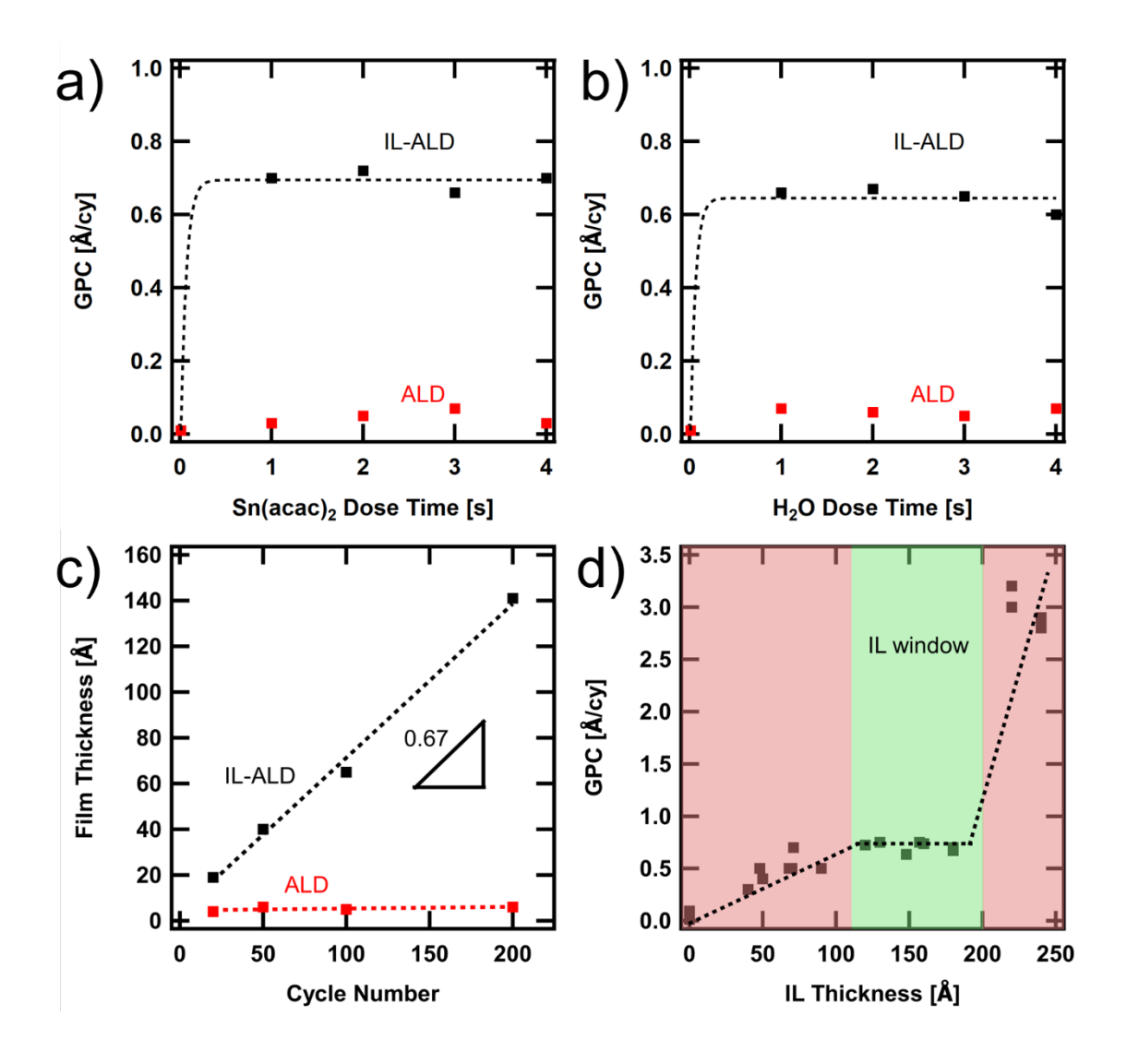


Figure 1: Saturation curve of the SnO ALD process as a function of (a) Sn(acac)₂ dose time, and (b) water dose time. (c) Growth curve for IL-ALD process, showing linear growth behavior up to 200 cycles at a growth per cycle (GPC) of 0.67 Å/cycle. (d) GPC as a function of IL thickness, showing a central region of constant growth. Data points shown in black are ALD processes with IL and points shown in red are traditional ALD processes without IL. Dashed curves and dotted lines in (a), (b), (d) are guides to the eye. Dotted lines in (c) are a result of a two-parameter least-squares linear regression fit.

Analysis of IL-ALD films. We performed XPS to determine the elemental composition and oxidation state information of the IL-ALD films grown with Sn(acac)₂ and water. Previously, ALD of tin oxide using tin acetylacetonate had only been reported using ozone, which deposited a film of SnO₂ with a Sn oxidation state of +4.³⁹ Due to the highly oxidizing nature of ozone, the Sn(II) metal center in tin acetylacetonate oxidizes to Sn(IV) during the deposition process with ozone. However, it was not known a priori what Sn oxidation state might form in a process using water as a counter-reactant, as in the gentler IL process used in this work.

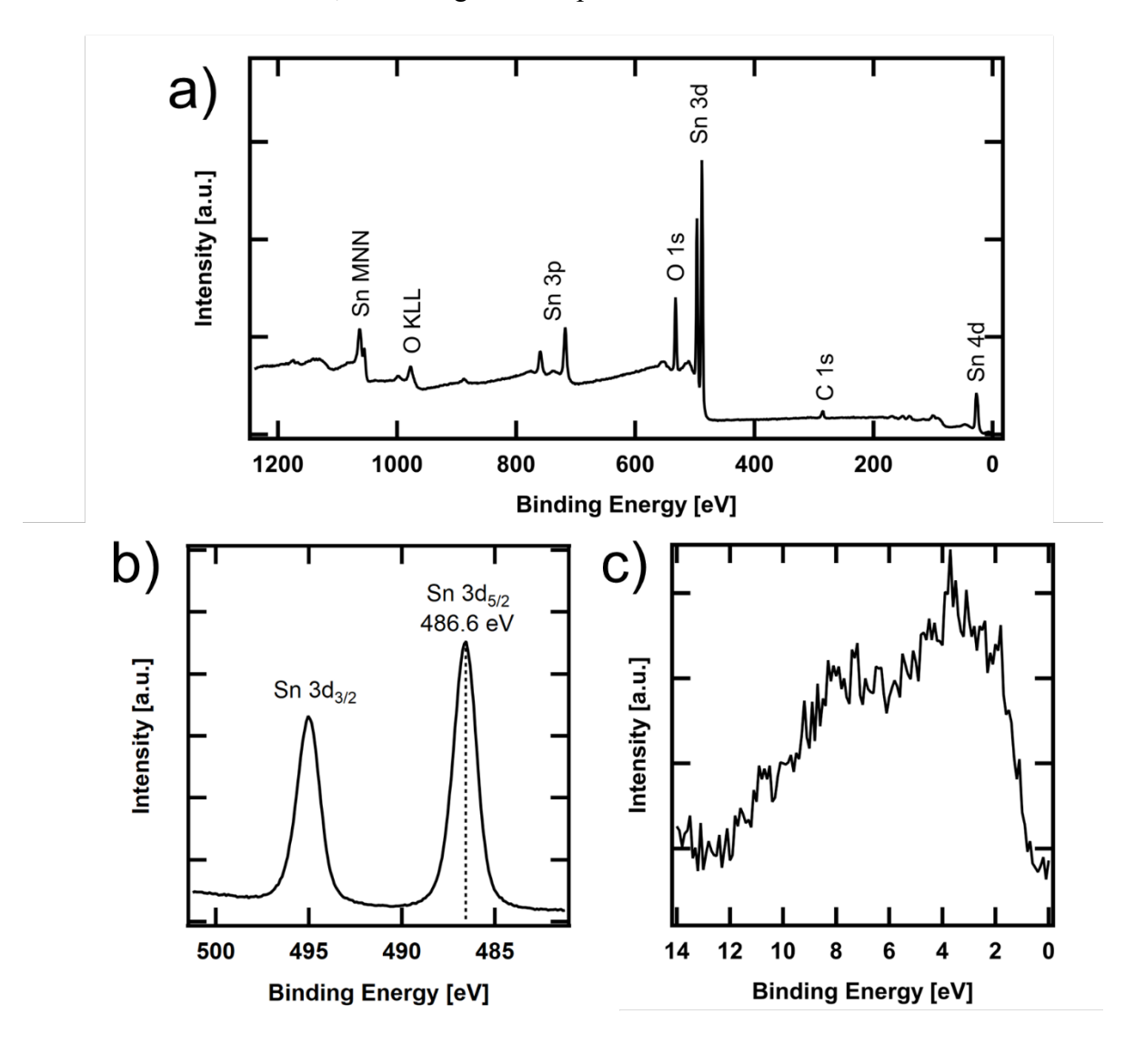


Figure 2: (a) XPS survey scan of IL-ALD tin oxide film. (b) XPS Sn 3d high-resolution scan. (c) XPS valence band spectrum. The sample used in these measurements was 100 Å thick.

Shown in Figure 2a, the XPS survey scan reveals the presence of tin oxide with minor carbon contamination. We note that due to the ex-situ nature of this XPS measurement, there will be adventitious carbon contamination. The high-resolution region of Sn 3d is shown in Figure 2b. but because Sn(II) and Sn(IV) are very similar in XPS binding energy (486.5 eV vs 486.7 eV). we used two other methods to determine the oxidation state of the tin. First, we determined the elemental ratios in the high resolution XPS spectra. The measured Sn:O ratio of 45:55 ratio suggests that the nominal composition of our IL-ALD film is $SnO_{1+\delta}$, i.e., nearly SnO with slight non-stoichiometry. Next, we measured the valence band XPS spectra of the IL-ALD film, with results shown in Figure 2c. Because SnO and SnO₂ have different electronic band structures. their valence band XPS spectra are different, ^{72,73} so we can use this region of the XPS spectrum as a fingerprint to corroborate the tin oxide stoichiometry. By referencing literature spectra for SnO⁷³ and SnO₂ as shown in SI Figure S3,⁷² it is evident that the valence spectrum best matches that for SnO. Notably, the onset of the first peak at low binding energies in the valence band spectra of the IL-ALD film occurs near 0 eV, which is indicative of SnO and not SnO₂. This result is reasonable since the tin precursor originally exists as Sn(II) and because water is not an oxidizing counter-reactant. Furthermore, as discussed next, in the proposed solvent-mediated reaction mechanism, the water acts solely as a nucleophile and not as an oxidant.

Reaction mechanism between Sn(acac)₂ and H₂O. The mechanism of the reaction between tin acetylacetonate precursor and the water counter-reactant in the IL is important to establish. We

can look to literature results of other metal acetylacetonates with water to understand likely reaction pathways, making comparisons between what takes place in the gas-phase versus in solution. First, in vapor-phase reactivity studies of metal acetylacetonates, chromatography-mass spectrometry (GM-MS) of various metal acetylacetonates^{74–76} showed that the entire acetylacetonate ligand is exchanged during reaction as acetylacetone. However, because acetylacetonate is a very strong chelating ligand and thus bound tightly to the metal center, this ligand exchange reaction does not take place until temperatures above 300 °C. Furthermore, these gas-phase reactivity studies were done with co-flow of both the metal acetylacetonate and water at once, which resembles a CVD process rather than an ALD one. In particular, in the reactions of Ni(acac)₂ (300 °C),⁷⁵ Co(acac)₂ (310 °C),⁷⁵ and Cu(acac)₂ (432 °C)⁷⁶ with water, acetylacetone (Hacac) is produced as a product of the ligand exchange reaction at these elevated temperatures. At a lower reaction temperature of 100 °C, as in our process, this type of reaction has not been demonstrated to occur at appreciable rates in vapor-phase.⁷⁶

Even though the previous reports on metal acetylacetonate precursors were performed under CVD-like conditions, because ligand exchange chemistry is so prevalent in ALD, it is perhaps still reasonable to expect this reaction mechanism to permit ALD of metal oxides from metal acetylacetonates and water. The mechanism of full ligand exchange is depicted in Figure 4b. Yet, successful reports of metal acetylacetonate ALD processes with water are scarce, likely because at lower deposition temperatures, this ligand exchange reaction is kinetically prohibitive. For example, in a previous study on tin acetylacetonate ALD processes, ³⁹ it was reported that water was insufficiently reactive as a counter-reactant even at 375 °C, and an ozone counter-reactant was required for any growth to occur. Similarly, we did not see significant deposition in our studies with Sn(acac)₂ and H₂O in the absence of the ionic liquid. However, we did see

deposition in the presence of the IL, and consequently we expect the operative reaction mechanism in IL-ALD to be different than simple ligand exchange.

To investigate the reaction mechanism operative within the IL-ALD process, we first performed the reaction directly in a bulk IL solution as a reference. We prepared the reaction mixture as described in the Methods section to mimic the reaction conditions as closely as possible. We then used NMR to detect reaction species post-reaction. Figure 3a,b shows the ¹³C and ¹H NMR spectra collected, respectively. Looking first at the ¹³C results, the spectrum shows peaks that correspond to both acetone and acetic acid, labeled as molecule A and B respectively. The peak shifts, assignments, and literature references are described in SI Section A. In particular, there are two extremely deshielded carbons that correspond to the carbonyl carbon on both acetone and acetic acid. There are also two aliphatic carbons that are attributed to acetone and acetic acid. Of note, the ¹³C shift for acetate at 191.76 ppm is quite downfield from free acetic acid which typically occurs as 178 ppm in CDCl₃; this shift is attributed to metal-chelating carboxylates, 77–79 a binding configuration which is possible in our system due to the presence of tin ions. Next, the ¹H spectrum reveals signatures of acetone and acetic acid as well, again labeled as molecules A and B. The NMR spectra also contain multiple peaks that correspond to the solvent, which is the EMIM HSO₄ IL and D₂O. We do not expect to detect the acidic proton in acetic acid because of rapid proton exchange with deuterium present in D₂O, which is not NMR active.

Most notably, in the NMR spectra we do not see either intact tin acetylacetonate or acetylacetone, which have unique characteristic peaks near 100 ppm in the ¹³C NMR spectrum and 5.52 ppm in a ¹H NMR spectrum, as labeled in Figure 3a,b.^{53,54} The absence of acetylacetone

suggests two main characteristics about the IL-mediated reaction mechanism: 1) the mechanism is different than the higher temperature, gas phase mechanism, since acetylacetonate is known to undergo ligand exchange to form intact acetylacetone in the gas phase in that process, and 2) the mechanism likely breaks up the acetylacetonate ligand during the process since acetylacetonate is absent in the NMR spectrum.

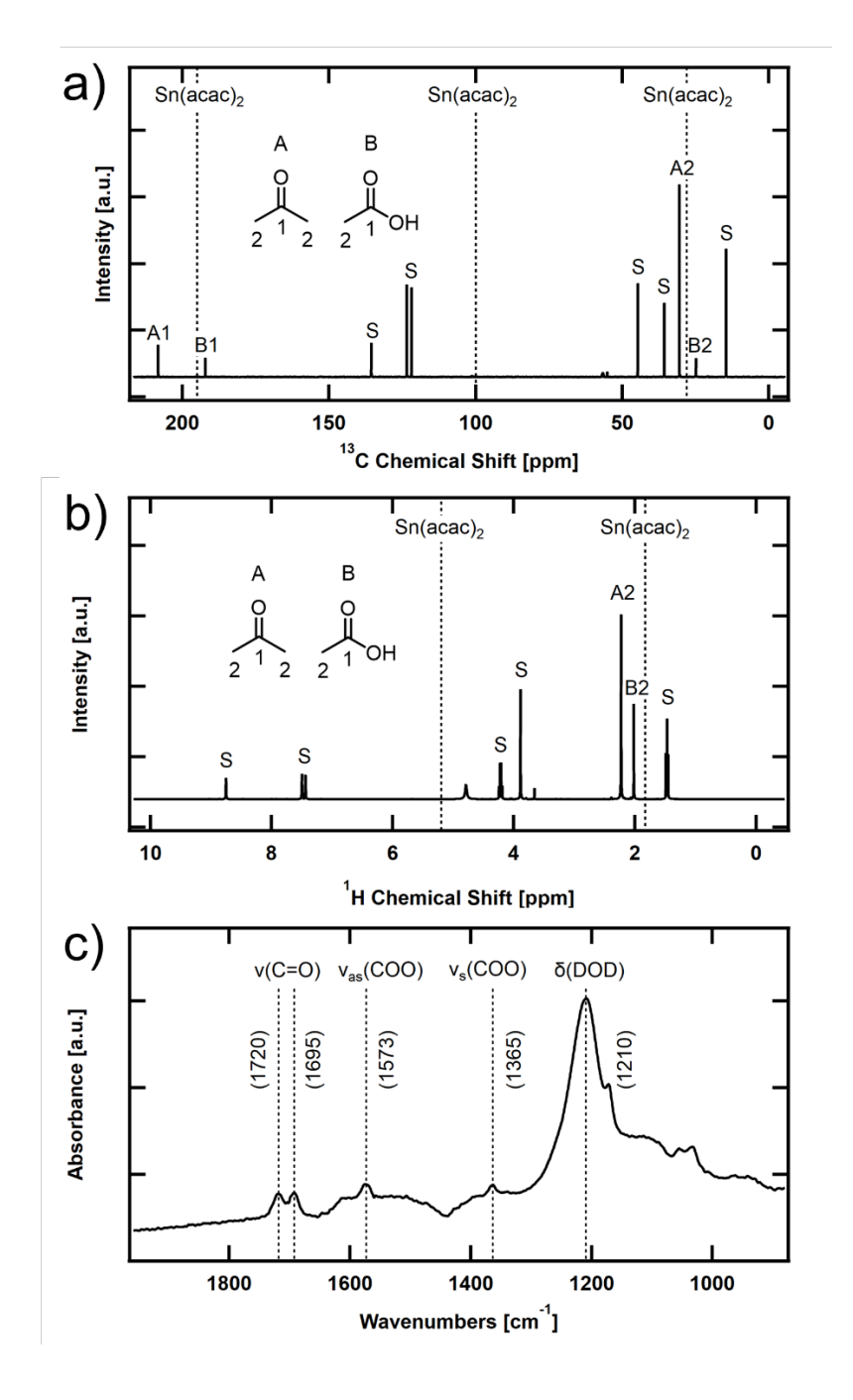


Figure 3: (a) ¹³C and (b) ¹H NMR for reaction products of tin acetylacetonate and D₂O in EMIM HSO₄. Peak assignments are in SI section A and also labeled in the spectra, with A1 and A2 corresponding to acetone peaks, B1 and B2 corresponding to acetic acid peaks, and S corresponding to solvent peaks. (c) IR spectrum of the same reaction products of tin acetylacetone and water in EMIM HSO₄ and D₂O. Key peak positions given in wavenumbers are shown in parentheses on the figure.

We also compare the NMR results with FTIR spectroscopy analysis of the reaction products, shown in Figure 3c. The peak assignments are tabulated and show with reference peak assignments in SI Table S1. Here, we also observe the presence of carbonyl functional groups through peaks at 1720 and 1695 cm⁻¹, which are consistent with acetic acid and acetone, respectively. The appearance of both the symmetric and asymmetric stretching modes of a carboxylate at 1573 and 1365 cm⁻¹ is also consistent with acetic acid, since it is in acid-base equilibrium with the acetate form. However, since FTIR spectroscopy is less analytic in practice compared to NMR analysis of small molecules, we use this FTIR analysis only as corroborating evidence to the conclusions made via NMR.

We propose that the presence of these two species suggests an addition-elimination reaction mechanism of the acetylacetonate ligand with water in which a C-C bond in acetylacetonate is broken to form acetone and acetic acid; this type of reaction mechanism has been observed in the solvent-facilitated reaction of metal acetylacetonates with amines⁵⁴ and alcohols.⁵³ We hypothesize that the same addition-elimination mechanism is operating in the current reaction with water as the nucleophile, as shown in Figure 4a. This reaction mechanism

involves a C-C bond cleavage of the acetylacetonate ligand, which is typically energetically unfavorable. In fact, literature has reported that when acetylacetone (Hacac) was refluxed with 1-butanol or isobutanol to determine its stability,⁵³ no alcoholysis was observed after 24 hours of reflux, suggesting that free acetylacetone is stable to reaction with alcohol nucleophiles.

However, it is known that when acetylacetonate is chelated to metal ions, taking the acetylacetonate form, it becomes more reactive towards nucleophiles,⁵³ whereby the metal ion activates the acetylacetonate ligand. Our hypothesized reaction mechanism in Figure 4a is consistent with the addition-elimination mechanism that has been reported for other metal acetylacetonates with amines and alcohols, but in this case water serves as the nucleophile.

Consistent with the mechanism involving water instead of an alcohol or an amine, acetic acid is produced as the first byproduct rather than esters and amides. Acetone is produced in all three mechanisms (i.e., with water, amines, or alcohols) as the second byproduct. This proposed reaction mechanism is in agreement with the observed reaction products by NMR and IR.

The proposed mechanism can also help explain why the solvent-mediated reaction (Figure 4a) is possible at lower temperatures compared to the vapor-phase, ligand-exchange mechanism (Figure 4b). The chelate effect mentioned above suggests that acetylacetonate is very strong bonded to Sn(II), making it difficult to remove by ligand exchange. However, if water can initiate the addition-elimination reaction to cleave the C-C bond in acetylacetonate rather than simple ligand exchange, then the bidentate nature of acetylacetone is lost when it forms the two separate products of acetone and acetic acid. Although acetate, the deprotonated form of acetic acid, is also a bidentate ligand, it is not nearly as strongly binding a ligand as acetylacetonate;⁸⁰ moreover, the acid-base equilibrium of acetic acid means that acetate is not present in the same stoichiometric concentration as acetylacetonate. The Hammett acidity function, H₀, of the IL

used in this study, EMIM HSO₄, is 1.94⁸¹. This value suggests that acetic acid, which possesses a pKa of 4.76, should be primarily in the protonated form, which is a more weakly chelating ligand than the deprotonated form due to the lack of negative charge.

a)
$$\xrightarrow{H_2O}$$
 $\xrightarrow{H_2O}$ \xrightarrow

Figure 4: (a) Proposed addition-elimination reaction mechanism between tin acetylacetonate and water in solvent. (b) Established ligand-exchange reaction mechanism^{75,76} between metal acetylacetonate and water in vapor-phase, typically at high temperatures.

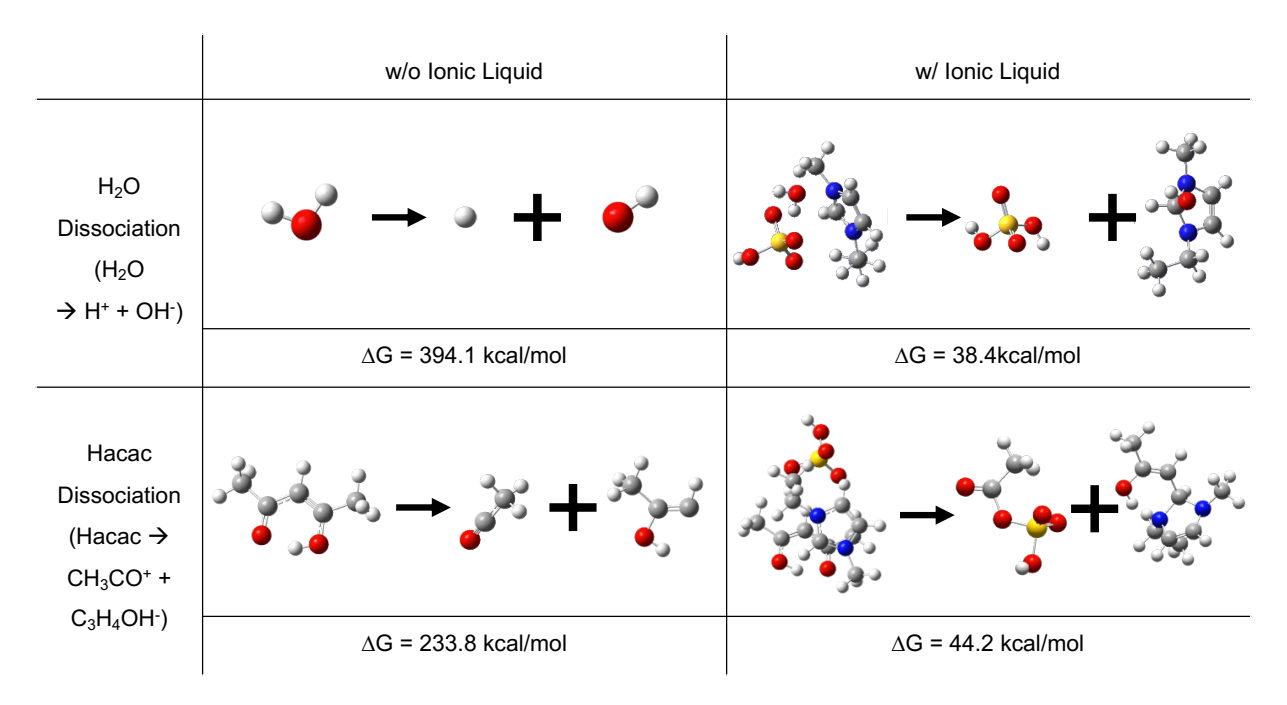


Figure 5. Bond dissociation energies of H₂O and Hacac with or without ionic liquid. All geometries optimized with DFT calculation. (red=oxygen, white=hydrogen, grey=carbon, blue=nitrogen, yellow=sulfur)

To further probe the feasibility of the proposed addition-elimination mechanism, we investigated the effect of an IL on dissociation of H₂O and on C-C cleavage of Hacac using DFT calculations. Both the O-H and C-C bonds must be dissociated in the mechanism illustrated in Figure 4a. As shown in Figure 5, 394.1 kcal/mol of energy is required to dissociate H₂O into H⁺ and OH⁻ without the IL, a formidably high value. On the other hand, in the presence of the IL, which is simulated as a single EMIM-HSO₄ complex, a much lower energy of 38.4 kcal/mol is required to dissociate H₂O. Since the EMIM of the IL has a positive charge and the HSO₄ has a negative charge, it can be inferred that the polarity of IL helps the dissociation of H₂O. This polarity of the IL leads to similar results in the dissociation of Hacac. To cleave the C-C bond in Hacac, 233.8 kcal/mol of energy is required without the IL. However, with the IL, a much lower energy of only 44.2 kcal/mol is required. Consequently, the results of the DFT calculations help

support the conclusion that the presence of the IL is involved in the dissociation of H₂O and the C-C bonds in the acac ligand, making it easier for the reaction to occur.

Ligand modification mechanism: non-ligand preserving chemistry. With both the experimental and theoretical results supporting the presence of an addition-elimination mechanism in the IL-ALD of SnO, we next turn to understand how this reaction mechanism fits into the context of known thermal ALD reactions. Generally, four classes of reaction mechanisms for thermal ALD have been identified: ligand exchange, associative adsorption, dissociative adsorption, and oxidation. Furthermore, we can differentiate the latter mechanism class from the former three by its non-ligand preserving nature. That is, an ALD reaction mechanism which occurs by oxidation does not preserve the chemical functionality of the ligand being modified, since the ligand is oxidized during the reaction process. This can be seen in the reaction byproduct differences between the ALD of trimethylaluminum (TMA) and water versus ALD of TMA and ozone to form alumina. In the water ALD case, ligand exchange occurs and methane is formed as a byproduct, so that the methyl ligands are preserved. In contrast, when ozone is used as the reactant, the methyl ligands are oxidized to CO and CO₂, thus following a "non-ligand preserving" mechanism.

With these differentiators, we can see that the addition-elimination mechanism we identify in our Sn(acac)₂ and water reaction also falls within this non-ligand preserving class. However, although this addition-elimination mechanism is non-ligand preserving, it is not an oxidation mechanism. Since water is used as the counter-reactant, the acetylacetonate ligand that is being altered does not undergo oxidation. Rather, because the acetylacetonate ligand is being modified and cleaved to form acetone and acetic acid, the ligand is dissociated but not oxidized.

Hence, we define a new and more general class of reaction mechanisms in ALD as "ligand modification", which encompasses both the previously-identified oxidation pathway as well as other non-oxidative non-ligand preserving mechanisms like the addition-elimination process introduced here.

IL-ALD growth mechanism. In typical ALD schemes, the growth process is described as occurring by a sequence of layer-by-layer, self-limiting gas-surface reactions. Due to the introduction of the ionic liquid layer, we investigated whether the ALD growth mechanism is still both self-limiting and comprised only of surface (not bulk) reactions. In traditional ALD, the surface reactions take place at the substrate-vapor interface, where the presence of functionalization (typically -OH functional groups) allow for the reaction to occur. By coating our substrates with the ultrathin layer of IL, we hope to modify the surface energetics of the desired reaction, by allowing the reaction to take place at the solid-solvent substrate-IL interface instead.

To probe the self-limiting nature, we can consider the saturation experiments in which we fixed the exposure of one precursor and varied the exposure of the other. If the reaction is self-limiting even in the presence of the IL, then the GPC should reach a constant value as a function of increasing precursor pulse time. From Figure 1a,b, it is evident that the GPC is saturating for both Sn(acac)₂ and water precursors, meaning the reactions are indeed self-limiting.

There are three reasonable locations where the SnO film growth may take place: at the substrate-IL interface, within the IL layer itself, and at the IL-vapor interface. To probe whether the reactions occur exclusively at the substrate-IL interface, we need to rule out the alternative

possibilities. Growth at the IL-vapor interface is not likely because our SnO films remain adhered to the Si substrate even after water sonication to remove the IL. If the SnO films grew at the IL-vapor interface, sonication and removal of the IL would also remove the SnO film. Furthermore, the XPS depth profile results shown in Figure 6a reveals that the IL layer is located above the SnO film rather than below it. The other possibility is that the ALD reactions are also taking place inside the bulk of the IL. This type of growth could occur if one precursor were retained within the IL upon dosing of the subsequent complementary precursor due to insufficient purging time. Such a CVD-like growth mechanism would be a function of the IL thickness, since a thicker ionic liquid layer would not only have the larger capacity to retain absorbed molecules but those precursors would also be harder to purge away. The growth studies performed in Figure 1d rule out the possibility of bulk growth when operating within the IL window: specifically, the GPC of SnO is nearly constant when the IL thickness is varied between 120 and 200 Å. On the other hand, once the IL thickness is increased to ~230 Å, the GPC does increase. As in the previous work, ³³ we attribute this higher GPC in the SnO system to CVD-like bulk growth due to insufficient purging. At lower IL thicknesses below 120 Å, the IL layer dewetting during deposition prevents ideal growth. As long as the IL thickness is kept within the optimized range, bulk growth does not occur. This result is reasonable because the desired ALD reaction should take place wherever there are compatible reactive sites available. By allowing for sufficient purging of precursors out of the IL layer, we eliminate the presence of these reactive sites from the IL layer so that they are only present at the substrate-IL interface.

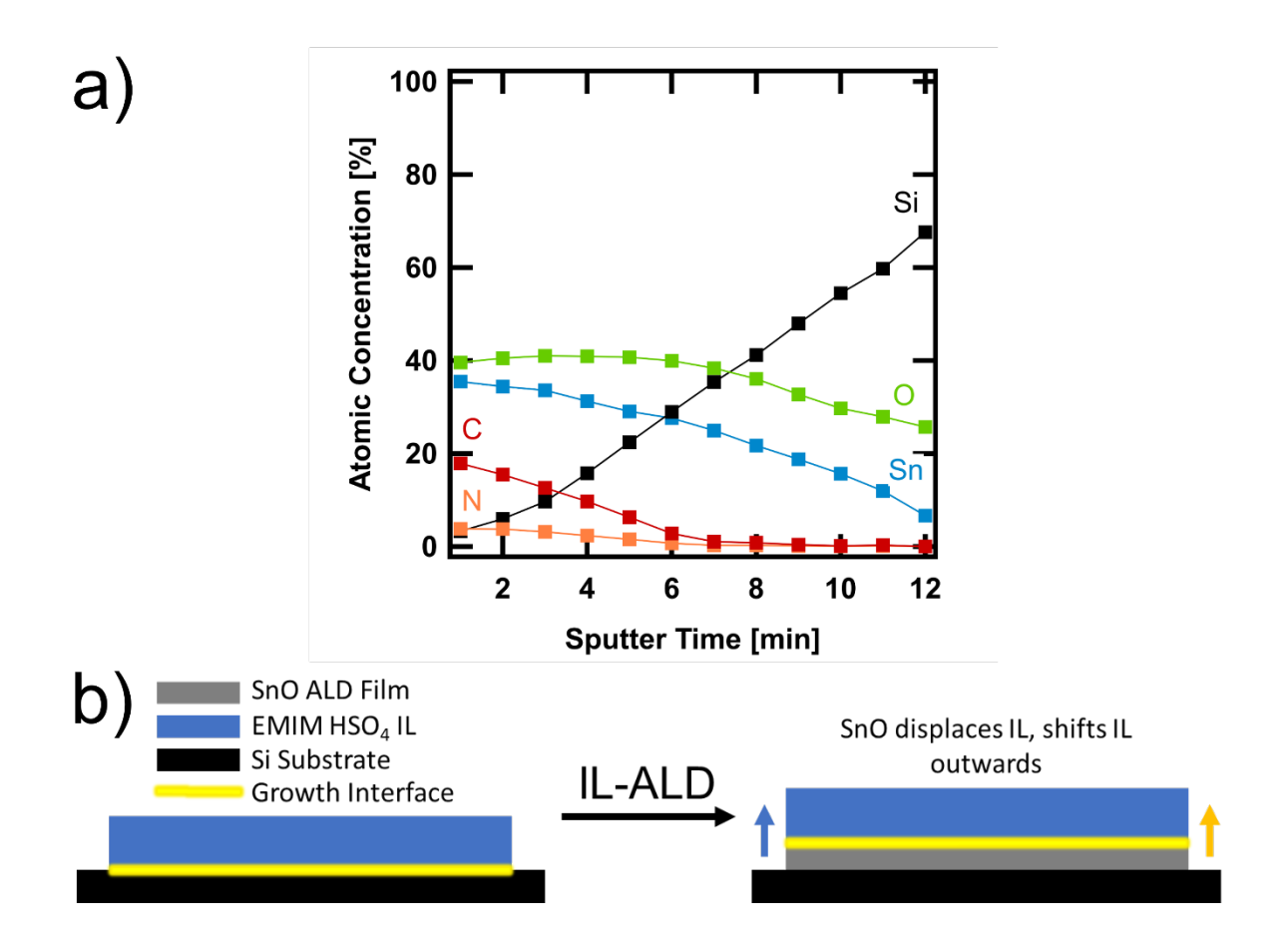


Figure 6: (a) XPS depth profile of an IL-ALD SnO deposition sample to investigate the location of the EMIM HSO₄ IL layer after deposition, which is tracked via the C and N signals. The sum of all 5 atomic compositions measured is fixed at 100%. (b) Proposed IL-ALD growth mechanism of SnO in an ionic liquid layer, in agreement with the observed XPS depth profile in (a). In the mechanism, the SnO layer displaces the IL layer that is initially present directly on the Si substrate, pushing the IL outward and leaving the ALD film at the Si substrate.

Elemental depth profiling was performed to shed further light on the IL-ALD growth mechanism. In this experiment, the elemental composition of the SnO and IL layers on Si was measured using XPS as a function of depth with sputtering. Prior to SnO ALD, the sample

contains a conformal IL layer of EMIM HSO₄ on the Si substrate. Once the SnO is grown, the relative positions of the IL layer and the SnO need to be determined. In principle, the SnO layer could be (1) between the IL layer and Si (interface growth), (2) within the IL layer itself (bulk growth), or (3) on top of the IL layer (surface growth). In our previous IL-MLD studies of the growth of PEKK, we determined that the MLD film sat between the IL layer and the substrate, i.e., scenario (1).³³ With sufficient purging for the given IL thickness, we avoided (2), and with correct choice of the IL layer to be inert with the precursors used, we avoided growth of the thin film at the IL-vapor surface (3).⁸³

The resulting XPS depth profile for the SnO IL-ALD film in this work is shown in Figure 6a, in which the C 1s, N 1s, Sn 3d^{5/2}, O 1s, and Si 2p signals were measured. The N 1s and C 1s signals correspond directly to the EMIM HSO₄, since these two elements are only present in the IL layer, and not in SnO or the Si substrate. The N and C signals drop to the level of noise after ~7 min of sputtering, as the signal from the underlying Si substrate begins to rise. On the other hand, the Sn and O signals continue to be detected throughout the sputtering process. The fact that XPS elemental signals attributed to SnO are still detected after those attributed to the IL are completely gone suggests that the EMIM HSO₄ layer is located on top of the SnO film. Hence, the depth profile results are consistent with scenario (1), in which the SnO layer is between the IL layer and Si substrate, and in agreement with the results from the IL-MLD system.³³ While the depth profile results by themselves do not rule out contribution from scenario (2), since signals attributed to SnO and the IL are both observed at the beginning of the sputtering process, the GPC studies in Figure 1d indicate that bulk growth is not occurring. Hence, the results support the conclusion that the IL-ALD process proceeds primarily by reaction at the ILsubstrate interface. As shown in the schematic of Figure 6b, in the proposed growth mode, the

SnO layer displaces the IL layer that is initially present directly on the Si substrate, pushing the IL outward and leaving the ALD film at the Si substrate. The SnO ALD film remains tethered to the Si substrate due to the formation of Si-SnO bonds during the first few cycles of the ALD process.

Conclusions

The process of ionic liquid assisted atomic layer deposition (IL-ALD) has been successfully demonstrated with the deposition of tin oxide. The SnO films were grown using tin acetylacetonate and water as precursors with a GPC of 0.67 Å/cycle at a deposition temperature of 100 °C, in a reaction enabled by an ultrathin layer of the ionic liquid 1-ethyl-3methylimidazolium hydrogen sulfate. The IL-ALD SnO process introduced here demonstrated the essential properties of ALD: linear and saturating growth, and self-limiting surface reactions. Characterization of the tin oxide films revealed a stoichiometry of Sn(II) oxide, distinct from ozone-based ALD using the Sn(acac)₂ precursor which deposits the Sn(IV) oxide. The solventmediated reaction mechanism was explored via ¹H NMR, ¹³C NMR, and FTIR spectroscopy of the reaction products: an addition-elimination mechanism was proposed whereby the water acts as a nucleophile, reacting with the acetylacetonate ligand and cleaving a C-C bond. As a result, this study introduces a new general type of ALD reaction mechanism, which we term ligandmodification, made possible via a solution-mediated pathway. DFT showed that the presence of the ionic liquid is beneficial to the proposed solvent-mediated mechanism by lowering the C-C bond cleavage energy compared to the mechanism solely in the vapor phase. Along with our previous study of the IL-MLD of PEKK, this proof-of-concept demonstration of the IL-ALD of SnO from tin acetylacetonate shows that the ionic liquid layer approach allows solvent-mediated reaction mechanisms to take place in ALD. This technique provides a new optimization direction Accepted for Publication, Journal of the American Chemical Society

for the development of novel ALD and MLD processes, enabling the manipulation of the energetics of surface reactions which has traditionally been limited in scope.

Supporting Information

The supporting Information is available free of charge at []. Spin curve for ionic liquid coating layer, XPS survey spectrum of ionic liquid layer, XPS valence band spectrum with comparisons to literature spectra of SnO and SnO₂, AFM of ionic liquid layer, and detailed NMR and IR peak assignments of products.

Acknowledgements

This work was supported by the National Science Foundation (Grant CHE-1904108). J. Shi acknowledges support from an NSF Graduate Research Fellowship (Grant DGE-1656518). Part of this work was performed at the Stanford Nano Shared Facilities (SNSF), supported by the National Science Foundation (Grant ECCS-1542152).

References

- (1) Chen, I. F.; Lu, C. F.; Su, W. F. Highly Conductive 2D Metal-Organic Framework Thin Film Fabricated by Liquid-Liquid Interfacial Reaction Using One-Pot-Synthesized Benzenehexathiol. *Langmuir* **2018**, *34*, 15754–15762.
- (2) Saifullah, M. S. M.; Khan, M. Z. R.; Hasko, D. G.; Leong, E. S. P.; Neo, X. L.; Goh, E. T. L.; Anderson, D.; Jones, G. A. C.; Welland, M. E. Spin-Coatable HfO2 Resist for Optical and Electron Beam Lithographies. *J. Vac. Sci. Technol. B, Nanotechnol. Microelectron. Mater. Process. Meas. Phenom.* 2010, 28, 90–95.

- (3) Cha, S. H.; Oh, M. S.; Lee, K. H.; Im, S.; Lee, B. H.; Sung, M. M. Electrically Stable Low Voltage ZnO Transistors with Organic/Inorganic Nanohybrid Dielectrics. *Appl. Phys. Lett.* **2008**, *92*, 023506.
- (4) Chae, M. G.; Han, S. H.; Park, B. K.; Chung, T. M.; Han, J. H. Atomic-Layer-Deposited SnO Film Using Novel Sn(Dmamb)2 Precursor for p-Channel Thin Film Transistor. *Appl. Surf. Sci.* **2021**, *547*, 0–4.
- (5) Asundi, A. S.; Hoffman, A. S.; Bothra, P.; Boubnov, A.; Vila, F. D.; Yang, N.; Singh, J. A.; Zeng, L.; Raiford, J. A.; Abild-Pedersen, F.; Bare, S. R.; Bent, S. F. Understanding Structure–Property Relationships of MoO3–Promoted Rh Catalysts for Syngas Conversion to Alcohols. *J. Am. Chem. Soc.* 2019, 141, 19655–19668.
- (6) Singh, J. A.; Hoffman, A. S.; Schumann, J.; Boubnov, A.; Asundi, A. S.; Nathan, S. S.; Nørskov, J.; Bare, S. R.; Bent, S. F. Role of Co₂ C in ZnO-Promoted Co Catalysts for Alcohol Synthesis from Syngas. *ChemCatChem* 2019, 11, 799–809.
- (7) Yang, N.; Liu, X.; Asundi, A. S.; Nørskov, J. K.; Bent, S. F. The Role of Sodium in Tuning Product Distribution in Syngas Conversion by Rh Catalysts. *Catal. Letters* 2018, 148, 289–297.
- (8) Yan, H.; Lin, Y.; Wu, H.; Zhang, W.; Sun, Z.; Cheng, H.; Liu, W.; Wang, C.; Li, J.; Huang, X.; Yao, T.; Yang, J.; Wei, S.; Lu, J. Bottom-up Precise Synthesis of Stable Platinum Dimers on Graphene. *Nat. Commun.* **2017**, *8*, 1–10.
- (9) Piernavieja-Hermida, M.; Lu, Z.; White, A.; Low, K. Bin; Wu, T.; Elam, J. W.; Wu, Z.; Lei, Y. Towards ALD Thin Film Stabilized Single-Atom Pd1 Catalysts. *Nanoscale* 2016, 8, 15348–15356.
- (10) Ramos Ferrer, P.; Mace, A.; Thomas, S. N.; Jeon, J.-W. Nanostructured Porous Graphene

- and Its Composites for Energy Storage Applications. Nano Converg. 2017, 4, 29.
- (11) Guo, M.; Zhang, M.; He, D.; Hu, J.; Wang, X.; Gong, C.; Xie, X.; Xue, Z. Comb-like Solid Polymer Electrolyte Based on Polyethylene Glycol-Grafted Sulfonated Polyether Ether Ketone. *Electrochim. Acta* **2017**, *255*, 396–404.
- (12) Xiong, F.; Wang, H.; Liu, X.; Sun, J.; Brongersma, M.; Pop, E.; Cui, Y. Li Intercalation in MoS2: In Situ Observation of Its Dynamics and Tuning Optical and Electrical Properties. *Nano Lett.* 2015, 15, 6777–6784.
- (13) Lee, J. Y.; Connor, S. T.; Cui, Y.; Peumans, P. Solution-Processed Metal Nanowire Mesh Transparent Electrodes. *Nano Lett.* **2008**, *8*, 689–692.
- (14) Luo, L.; Yang, H.; Yan, P.; Travis, J. J.; Lee, Y.; Liu, N.; Molina Piper, D.; Lee, S. H.; Zhao, P.; George, S. M.; Zhang, J. G.; Cui, Y.; Zhang, S.; Ban, C.; Wang, C. M. Surface-Coating Regulated Lithiation Kinetics and Degradation in Silicon Nanowires for Lithium Ion Battery. *ACS Nano* **2015**, *9*, 5559–5566.
- (15) Asundi, A. S.; Raiford, J. A.; Bent, S. F. Opportunities for Atomic Layer Deposition in Emerging Energy Technologies. *ACS Energy Lett.* **2019**, *4*, 908–925.
- (16) Raiford, J. A.; Belisle, R. A.; Bush, K. A.; Prasanna, R.; Palmstrom, A. F.; McGehee, M. D.; Bent, S. F. Atomic Layer Deposition of Vanadium Oxide to Reduce Parasitic Absorption and Improve Stability in N-i-p Perovskite Solar Cells for Tandems. *Sustain*. *Energy Fuels* 2019, 3, 1517–1525.
- (17) Lee, B. H.; Anderson, V. R.; George, S. M. Growth and Properties of Hafnicone and HfO2/Hafnicone Nanolaminate and Alloy Films Using Molecular Layer Deposition Techniques. *ACS Appl. Mater. Interfaces* **2014**, *6*, 16880–16887.
- (18) George, S. M. Atomic Layer Deposition: An Overview. Chem. Rev. 2010, 110, 111–131.

- (19) Aaltonen, T.; Alnes, M.; Nilsen, O.; Costelle, L.; Fjellvåg, H. Lanthanum Titanate and Lithium Lanthanum Titanate Thin Films Grown by Atomic Layer Deposition. *J. Mater. Chem.* **2010**, *20*, 2877–2881.
- (20) Weimer, M. S.; Kim, I. S.; Guo, P.; Schaller, R. D.; Martinson, A. B. F.; Hock, A. S. Oxidation State Discrimination in the Atomic Layer Deposition of Vanadium Oxides. *Chem. Mater.* **2017**, *29*, 6238–6244.
- (21) Nandi, D. K.; Sen, U. K.; Choudhury, D.; Mitra, S.; Sarkar, S. K. Atomic Layer Deposited Molybdenum Nitride Thin Film: A Promising Anode Material for Li Ion Batteries. *ACS Appl. Mater. Interfaces* **2014**, *6*, 6606–6615.
- (22) Becker, J. S.; Kim, E.; Gordon, R. G. Atomic Layer Deposition of Insulating Hafnium and Zirconium Nitrides. *Chem. Mater.* **2004**, *16*, 3497–3501.
- (23) Kozen, A. C.; Sowa, M. J.; Ju, L.; Strandwitz, N. C.; Zeng, G.; Babuska, T. F.; Hsain, Z.; Krick, B. A. Plasma-Enhanced Atomic Layer Deposition of Vanadium Nitride. *J. Vac. Sci. Technol. A* **2019**, *37*, 061505.
- (24) Jurca, T.; Moody, M. J.; Henning, A.; Emery, J. D.; Wang, B.; Tan, J. M.; Lohr, T. L.; Lauhon, L. J.; Marks, T. J. Low-Temperature Atomic Layer Deposition of MoS2Films. Angew. Chemie - Int. Ed. 2017, 56, 4991–4995.
- (25) Mane, A. U.; Letourneau, S.; Mandia, D. J.; Liu, J.; Libera, J. A.; Lei, Y.; Peng, Q.; Graugnard, E.; Elam, J. W. Atomic Layer Deposition of Molybdenum Disulfide Films Using MoF 6 and H 2 S. J. Vac. Sci. Technol. A Vacuum, Surfaces, Film. 2018, 36, 01A125.
- (26) Zeng, L.; Richey, N. E.; Palm, D. W.; Oh, I.-K.; Shi, J.; MacIsaac, C.; Jaramillo, T.; Bent,S. F. Modified Atomic Layer Deposition of MoS 2 Thin Films . J. Vac. Sci. Technol. A

- **2020**, *38*, 060403.
- (27) Kim, J. Y.; George, S. M. Tin Monosulfide Thin Films Grown by Atomic Layer Deposition Using Tin 2, 4-Pentanedionate and Hydrogen Sulfide. *J. Phys. Chem.* 2010, 114, 17597–17603.
- (28) Mackus, A. J. M.; Schneider, J. R.; Macisaac, C.; Baker, J. G.; Bent, S. F. Synthesis of Doped, Ternary, and Quaternary Materials by Atomic Layer Deposition: A Review. *Chem. Mater.* 2019, 31, 1142–1183.
- (29) Leng, C. Z.; Losego, M. D. Vapor Phase Infiltration (VPI) for Transforming Polymers into Organic–Inorganic Hybrid Materials: A Critical Review of Current Progress and Future Challenges. *Mater. Horiz.* **2017**, *4*, 747–771.
- (30) Losego, M. D.; Peng, Q. Atomic Layer Deposition and Vapor Phase Infiltration. Surf. Modif. Polym. Methods Appl. 2019, 135–159.
- (31) Petit, R. R.; Li, J.; Van de Voorde, B.; Van Vlierberghe, S.; Smet, P. F.; Detavernier, C. Atomic Layer Deposition on Polymer Thin Films: On the Role of Precursor Infiltration and Reactivity. *ACS Appl. Mater. Interfaces* **2021**, *13*, 46151–46163.
- (32) Richey, N. E.; De Paula, C.; Bent, S. F. Understanding Chemical and Physical Mechanisms in Atomic Layer Deposition. *J. Chem. Phys.* **2020**, *152*, 040902.
- (33) Shi, J.; Bent, S. F. Bridging the Synthesis Gap: Ionic Liquids Enable Solvent-Mediated Reaction in Vapor-Phase Deposition. *ACS Nano* **2021**, *15*, 3004–3014.
- (34) Bier, M.; Dietrich, S. Vapour Pressure of Ionic Liquids. Mol. Phys. 2010, 108, 211–214.
- (35) Hallett, J. P.; Welton, T. Room-Temperature Ionic Liquids: Solvents for Synthesis and Catalysis. 2. *Chem. Rev.* **2011**, *111*, 3508–3576.
- (36) Vafaeezadeh, M.; Alinezhad, H. Brønsted Acidic Ionic Liquids: Green Catalysts for

- Essential Organic Reactions. J. Mol. Liq. 2016, 218, 95–105.
- (37) Mehnert, C. P.; Cook, R. A.; Dispenziere, N. C.; Afeworki, M. Supported Ionic Liquid Catalysis A New Concept for Homogeneous Hydroformylation Catalysis. *J. Am. Chem. Soc.* **2002**, *124*, 12932–12933.
- (38) Kukawka, R.; Pawlowska-Zygarowicz, A.; Dzialkowska, J.; Pietrowski, M.; Maciejewski, H.; Bica, K.; Smiglak, M. Highly Effective Supported Ionic Liquid-Phase (SILP) Catalysts: Characterization and Application to the Hydrosilylation Reaction. ACS Sustain. Chem. Eng. 2019, 7, 4699–4706.
- (39) Kannan Selvaraj, S.; Feinerman, A.; Takoudis, C. G. Growth Behavior and Properties of Atomic Layer Deposited Tin Oxide on Silicon from Novel Tin(II)Acetylacetonate Precursor and Ozone. *J. Vac. Sci. Technol. A Vacuum, Surfaces, Film.* **2014**, *32*, 01A112.
- (40) Mandol, B.; Mahuli, N.; Ohno, K.; Scudder, L.; Sarkar, S. K. Atomic Layer Deposition of Chromium Oxide—An Interplay between Deposition and Etching. *J. Vac. Sci. Technol. A* 2021, 39, 032414.
- (41) De Ridder, M.; Van De Ven, P. C.; Van Welzenis, R. G.; Brongersma, H. H.; Helfensteyn, S.; Creemers, C.; Van Der Voort, P.; Baltes, M.; Mathieu, M.; Vansant, E. F. Growth of Iron Oxide on Yttria-Stabilized Zirconia by Atomic Layer Deposition. *J. Phys. Chem. B* 2002, 106, 13146–13153.
- (42) Zhou, K.; Huang, J. Q.; Zhang, Q.; Wei, F. Multi-Directional Growth of Aligned Carbon Nanotubes Over Catalyst Film Prepared by Atomic Layer Deposition. *Nanoscale Res. Lett.* **2010**, *5*, 1555–1560.
- (43) Utriainen, M.; Kröger-Laukkanen, M.; Niinistö, L. Studies of NiO Thin Film Formation by Atomic Layer Epitaxy. *Mater. Sci. Eng. B* **1998**, *B54*, 98–103.

- (44) Nilsen, O.; Balasundaraprabhu, R.; Monakhov, E. V.; Muthukumarasamy, N.; Fjellvåg,
 H.; Svensson, B. G. Thin Films of In2O3 by Atomic Layer Deposition Using In(Acac)3.
 Thin Solid Films 2009, 517, 6320–6322.
- (45) Hämäläinen, J.; Munnik, F.; Ritala, M.; Leskelä, M. Study on Atomic Layer Deposition of Amorphous Rhodium Oxide Thin Films. *J. Electrochem. Soc.* **2009**, *156*, D418.
- (46) Keränen, J.; Auroux, A.; Ek, S.; Niinistö, L. Preparation, Characterization and Activity Testing of Vanadia Catalysts Deposited onto Silica and Alumina Supports by Atomic Layer Deposition. *Appl. Catal. A Gen.* **2002**, *228*, 213–225.
- (47) Haukka, S.; Lakomaa, E. L.; Suntola, T. Chemisorption of Chromium Acetylacetonate on Porous High Surface Area Silica. *Appl. Surf. Sci.* **1994**, *75*, 220–227.
- (48) Backman, L. B.; Rautiainen, A.; Lindblad, M.; Krause, A. O. I. Effect of Support and Calcination on the Properties of Cobalt Catalysts Prepared by Gas Phase Deposition. *Appl. Catal. A Gen.* **2000**, *191*, 55–68.
- (49) Lindblad, M.; Lindfors, L. P.; Suntola, T. Preparation of Ni/Al2O3 Catalysts from Vapor Phase by Atomic Layer Epitaxy. *Catal. Letters* **1994**, *27*, 323–336.
- (50) Van Welzenis, R. G.; Bink, R. A. M.; Brongersma, H. H. A Mini-ALE Attachment to UHV Surface Analysis Equipment. *Appl. Surf. Sci.* **1996**, *107*, 255–259.
- (51) Nieminen, M.; Niinistö, L.; Rauhala, E. Growth of Gallium Oxide Thin Films from Gallium Acetylacetonate by Atomic Layer Epitaxy. *J. Mater. Chem.* **1996**, *6*, 27–31.
- (52) Elam, J. W.; Martinson, A. B. F.; Pellin, M. J.; Hupp, J. T. Atomic Layer Deposition of In
 2 O 3 Using Cyclopentadienyl Indium: A New Synthetic Route to Transparent Conducting
 Oxide Films. *Chem. Mater.* 2006, 18, 3571–3578.
- (53) Ambrožič, G.; Škapin, S. D.; Žigon, M.; Orel, Z. C. The Synthesis of Zinc Oxide

- Nanoparticles from Zinc Acetylacetonate Hydrate and 1-Butanol or Isobutanol. *J. Colloid Interface Sci.* **2010**, *346*, 317–323.
- (54) Pinna, N.; Garnweitner, G.; Antonietti, M.; Niederberger, M. A General Nonaqueous Route to Binary Metal Oxide Nanocrystals Involving a C-C Bond Cleavage. *J. Am. Chem. Soc.* **2005**, *127*, 5608–5612.
- (55) McNamara, W. R.; Snoeberger, R. C.; Li, G.; Schleicher, J. M.; Cady, C. W.; Poyatos, M.; Schmuttenmaer, C. A.; Crabtree, R. H.; Brudvig, G. W.; Batista, V. S. Acetylacetonate Anchors for Robust Functionalization of TiO2 Nanoparticles with Mn(II)-Terpyridine Complexes. J. Am. Chem. Soc. 2008, 130, 14329–14338.
- (56) Willis, A. L.; Chen, Z.; He, J.; Zhu, Y.; Turro, N. J.; O'Brien, S. Metal Acetylacetonates as General Precursors for the Synthesis of Early Transition Metal Oxide Nanomaterials. *J. Nanomater.* **2007**, *2007*, 014858.
- (57) Loscutoff, P. W.; Lee, H. B. R.; Bent, S. F. Deposition of Ultrathin Polythiourea Films by Molecular Layer Deposition. *Chem. Mater.* **2010**, *22*, 5563–5569.
- (58) Frisch, M. J.; Trucks, G. W.; Schlegel, H. B. Gaussian 16, Revision C.01. Gaussian, Inc.: Wallingford CT 2016.
- (59) Lee, C.; Yang, W.; Parr, R. G. Development of the Colle-Salvetti Correlation-Energy Formula into a Functional of the Electron Density. *Phys. Rev. B* **1988**, *37*, 785–789.
- (60) Becke, A. D. Density-functional Thermochemistry. III. The Role of Exact Exchange. *J. Chem. Phys.* **1993**, *98*, 5648–5652.
- (61) Weigend, F.; Ahlrichs, R. Balanced Basis Sets of Split Valence, Triple Zeta Valence and Quadruple Zeta Valence Quality for H to Rn: Design and Assessment of Accuracy. *Phys. Chem. Chem. Phys.* **2005**, *7*, 3297–3305.

- (62) Weigend, F. Accurate Coulomb-Fitting Basis Sets for H to Rn. *Phys. Chem. Chem. Phys.*2006, 8, 1057–1065.
- (63) Grimme, S.; Ehrlich, S.; Goerigk, L. Effect of the Damping Function in Dispersion Corrected Density Functional Theory. *J. Comput. Chem.* **2011**, *32*, 1456–1465.
- (64) Grimme, S.; Antony, J.; Ehrlich, S.; Krieg, H. A Consistent and Accurate Ab Initio Parametrization of Density Functional Dispersion Correction (DFT-D) for the 94 Elements H-Pu. *J. Chem. Phys.* **2010**, *132*, 154104.
- (65) Cossi, M.; Barone, V.; Cammi, R.; Tomasi, J. Ab Initio Study of Solvated Molecules: A New Implementation of the Polarizable Continuum Model. *Chem. Phys. Lett.* **1996**, *255*, 327–335.
- (66) Conrad Zhang, Z. Catalysis in Ionic Liquids. Adv. Catal. 2006, 49, 153–237.
- (67) Smith, E. L.; Abbott, A. P.; Ryder, K. S. Deep Eutectic Solvents (DESs) and Their Applications. *Chem. Rev.* **2014**, *114*, 11060–11082.
- (68) Zhang, S.; Zhang, J.; Zhang, Y.; Deng, Y. Nanoconfined Ionic Liquids. *Chem. Rev.* **2017**, 117, 6755–6833.
- (69) Gao, J.; Luedtke, W. D.; Landman, U. Layering Transitions and Dynamics of Confined Liquid Films. *Phys. Rev. Lett.* **1997**, *79*, 705–708.
- (70) Ori, G.; Villemot, F.; Viau, L.; Vioux, A.; Coasne, B. Ionic Liquid Confined in Silica Nanopores: Molecular Dynamics in the Isobaric-Isothermal Ensemble. *Mol. Phys.* **2014**, *112*, 1350–1361.
- (71) Borghi, F.; Milani, P.; Podestà, A. Solid-Like Ordering of Imidazolium-Based Ionic Liquids at Rough Nanostructured Oxidized Silicon Surfaces. *Langmuir* **2019**, *35*, 11881–11890.

- (72) Stranick, M. A.; Moskwa, A. SnO2 by XPS. Surf. Sci. Spectra 1993, 2, 50–54.
- (73) Stranick, M. A.; Moskwa, A. SnO by XPS. Surf. Sci. Spectra 1993, 2, 45–49.
- (74) Kytökivi, A.; Rautiainen, A.; Root, A. Reaction of Acetylacetone Vapour with γ-Alumina.
 J. Chem. Soc. Faraday Trans. 1997, 93, 4079–4084.
- (75) Weiss, T.; Zielasek, V.; Bäumer, M. Influence of Water on Chemical Vapor Deposition of Ni and Co Thin Films from Ethanol Solutions of Acetylacetonate Precursors. *Sci. Rep.*2015, 5, 1–13.
- (76) Nasibulin, A. G.; Shurygina, L. I.; Kauppinen, E. I. Synthesis of Nanoparticles Using Vapor-Phase Decomposition. *Colloid J.* **2005**, *67*, 1–20.
- (77) Faccini, F.; Fric, H.; Schubert, U.; Wendel, E.; Tsetsgee, O.; Müller, K.; Bertagnolli, H.; Venzo, A.; Gross, S. ω-Mercapto-Functionalized Hafnium- and Zirconium-Oxoclusters as Nanosized Building Blocks for Inorganic-Organic Hybrid Materials: Synthesis, Characterization and Photothiol-Ene Polymerization. *J. Mater. Chem.* 2007, 17, 3297–3307.
- (78) De Roo, J.; Baquero, E. A.; Coppel, Y.; De Keukeleere, K.; Van Driessche, I.; Nayral, C.; Hens, Z.; Delpech, F. Insights into the Ligand Shell, Coordination Mode, and Reactivity of Carboxylic Acid Capped Metal Oxide Nanocrystals. *Chempluschem* **2016**, *81*, 1216–1223.
- (79) Tolstoy, P. M.; Schah-Mohammedi, P.; Smirnov, S. N.; Golubev, N. S.; Denisov, G. S.; Limbach, H. H. Characterization of Fluxional Hydrogen-Bonded Complexes of Acetic Acid and Acetate by NMR: Geometries and Isotope and Solvent Effects. *J. Am. Chem.* Soc. 2004, 126, 5621–5634.
- (80) Grasdalen, H. Equilibria of Copper(II) Acetate with Acetylacetone in Acetic Acid and

- Methanol Solutions from Optical and Electron Spin Resonance Measurements. *J. Chem. Soc. Faraday Trans. 2 Mol. Chem. Phys.* **1973**, *69*, 462–470.
- (81) Liu, Y.; Wang, Y. T.; Liu, T.; Tao, D. J. Facile Synthesis of Fructone from Ethyl Acetoacetate and Ethylene Glycol Catalyzed by SO3H-Functionalized Brønsted Acidic Ionic Liquids. *RSC Adv.* **2014**, *4*, 22520–22525.
- (82) Goldstein, D. N.; McCormick, J. A.; George, S. M. Al 2O 3 Atomic Layer Deposition with Trimethylaluminum and Ozone Studied by in Situ Transmission FTIR Spectroscopy and Quadrupole Mass Spectrometry. *J. Phys. Chem. C* **2008**, *112*, 19530–19539.
- (83) Frank-Finney, R. J.; Bradley, L. C.; Gupta, M. Formation of Polymer-Ionic Liquid Gels Using Vapor Phase Precursors. *Macromolecules* **2013**, *46*, 6852–6857.

TOC Figure:

